

-Electronic Supplementary Information (ESI)-

All-alike hollow nanotubes of g-C₃N₄ Converting Photons into Fuel by Splitting Water

Mani Preeyanghaa, ^a Chitiphon Chuaicham, ^b Sulakshana Shenoy, ^b Bernaurdshaw

Neppolian, ^c Keiko Sasaki, ^{b*} Karthikeyan Sekar, ^{b,c*}

^a*Department of Physics and Nanotechnology, SRM Institute of Science and Technology,*

Kattankulathur, Chennai, 603203, India

^b*Department of Earth Resources Engineering, Faculty of Engineering, Kyushu University,*

744 Motooka, Nishiku, Fukuoka 819-0395, Japan

^c*Department of Chemistry, SRM Institute of Science and Technology, Kattankulathur,*

Chennai, 603203, India

*Corresponding Authors: Email: keikos@mine.kyushu-u.ac.jp; kart@mine.kyushu-u.ac.jp.

EXPERIMENTAL SECTION

Synthesis of HTC� and NSCN

All the raw materials were of analytical grade and used without further purification. Typically, the powders of urea and melamine were combined with oxalic acid (**Table S1**) and granulated uniformly using mortar and pestle. Subsequently, the precursor was transferred into a closed ceramic crucible and maintained at 520 °C for 2 h with a heating rate of 5 °C/min in a muffle furnace. After cooled to room temperature, the resulting material (denoted as HTC�(x)) was collected and granulated to a fine powder. For comparison, the pristine CN (denoted as NSCN) was also prepared by direct polymerization of urea as a precursor at 520 °C for 2 h.

Table S1. Synthesis of HTC�(x) by varying the proportion of N₂-rich CN precursors.

Urea (g)	Melamine (g)	Oxalic acid (g)	Sample yield (g)	Sample label
4	0.5	0.5	0.05	HTC�(1)
3.5	1	0.5	0.1	HTC�(2)
2.5	2	0.5	0.34	HTC�(3)
2	2.5	0.5	1.46	HTC�(4)
1.5	3	0.5	1.63	HTC�(5)
1	3.5	0.5	1.85	HTC�(6)

Characterization

The powder X-ray diffraction (XRD) patterns were acquired using a Cu K α radiation source on a Rigaku Ultima IV powder X-ray diffractometer. Fourier-transform infrared (FT-IR) spectra were obtained on the Jasco FTIR-670 Plus. X-ray photoelectron spectroscopy (XPS) spectra were carried out on a ULVAC-PHI ESCA 5800 XPS Microprobe with an Al K α excitation source. All spectra were corrected based on standard C1s peak at 284.6 eV. The morphology and elemental composition were examined using field emission scanning electron

microscopy (FE-SEM, ZEISS Ultra-55) and high-resolution transmission electron microscopy (HRTEM, JEOL JEM-2100HCKM). High-angle annular dark field scanning TEM (HAADF-STEM) coupled with energy dispersive spectroscopy (EDS) elemental mapping were also recorded. The multipoint Brunauer-Emmett-Teller (BET) and Barrett-Joyner-Halenda (BJH) were determined by BEL-Max N₂ porosimeter. A UV-vis spectrophotometer (Shimadzu UV-2450) was used to record UV-vis diffused reflectance (UV-DRS) spectra. The photoluminescence (PL) spectra were measured using a fluorescence spectrophotometer (JASCO F-6600).

Reversed double-beam photoacoustic spectroscopy (RDB-PAS)

A sample container containing ~200 mg of synthesized products was placed in a PAS cell equipped with an electret condenser microphone and quartz window on the upper side, which was infused with methanol-saturated N₂ gas for 30 min before being firmly closed. A grating monochromator attached to a Xe lamp was controlled at 80 Hz by a light chopper that transmitted a beam of light over the wavelength range of 650–350 nm via a cell window and the PA signal was monitored using a digital lock-in amplifier. Based on the amount of photoabsorption change for accumulated electrons, the energy-resolved distribution of electron traps (ERDT)/conduction-band bottom (CBB) patterns were measured for the synthesized samples.

Photoelectrochemical characterization

The Mott-Schottky, electrochemical impedance spectroscopy (EIS) and transient photocurrent (TPC) response of the synthesized products were measured using an Autolab potentiostat electrochemical workstation. A three-electrode cell system was used comprising a Pt wire counter electrode, Hg/Hg₂SO₄ reference electrode and glassy carbon (GC) working electrode in 0.5 M Na₂SO₄ electrolyte solution. The working electrode was prepared as follows: 5 mg synthesized product was uniformly dispersed in 0.5 mL Nafion containing 1:1 v/v of a

water/ethanol mixture. After 30 min of ultrasonication, 5 μ L of homogeneous colloidal solution was drop cast onto the GC electrode (3 mm diameter) and dried at ambient temperature. EIS Nyquist plots were recorded with a 10 mV AC signal in the frequency range of 100 kHz to 0.1 Hz. The light source used for measuring the TPC response was a 200 W Hg-Xe arc lamp.

Photocatalytic hydrogen production

Typically, 20 mg of synthesized products was uniformly dispersed in 50 mL of distilled water containing 10 vol% triethanolamine (TEOA) of sacrificial agent and 1 wt% Pt as cocatalysts using an ultrasonicator. Prior to UV-Vis light irradiation, the N₂ gas was continuously purged in a sealed quartz photoreactor for 30 min to remove all the dissolved oxygen from the reaction mixture. The evolved gas was collected in a 1 mL airtight syringe at a periodic interval and analysed using gas chromatography (Shimadzu Nexis GC-2030).

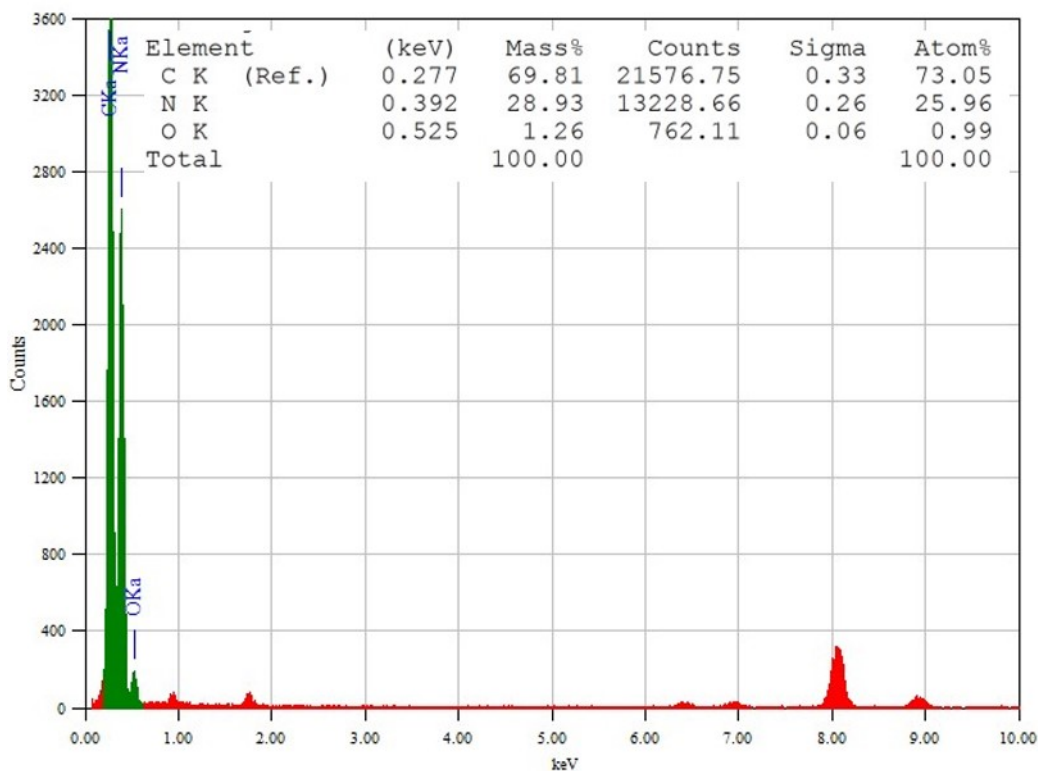


Fig. S1. EDS spectra of HTC/N.

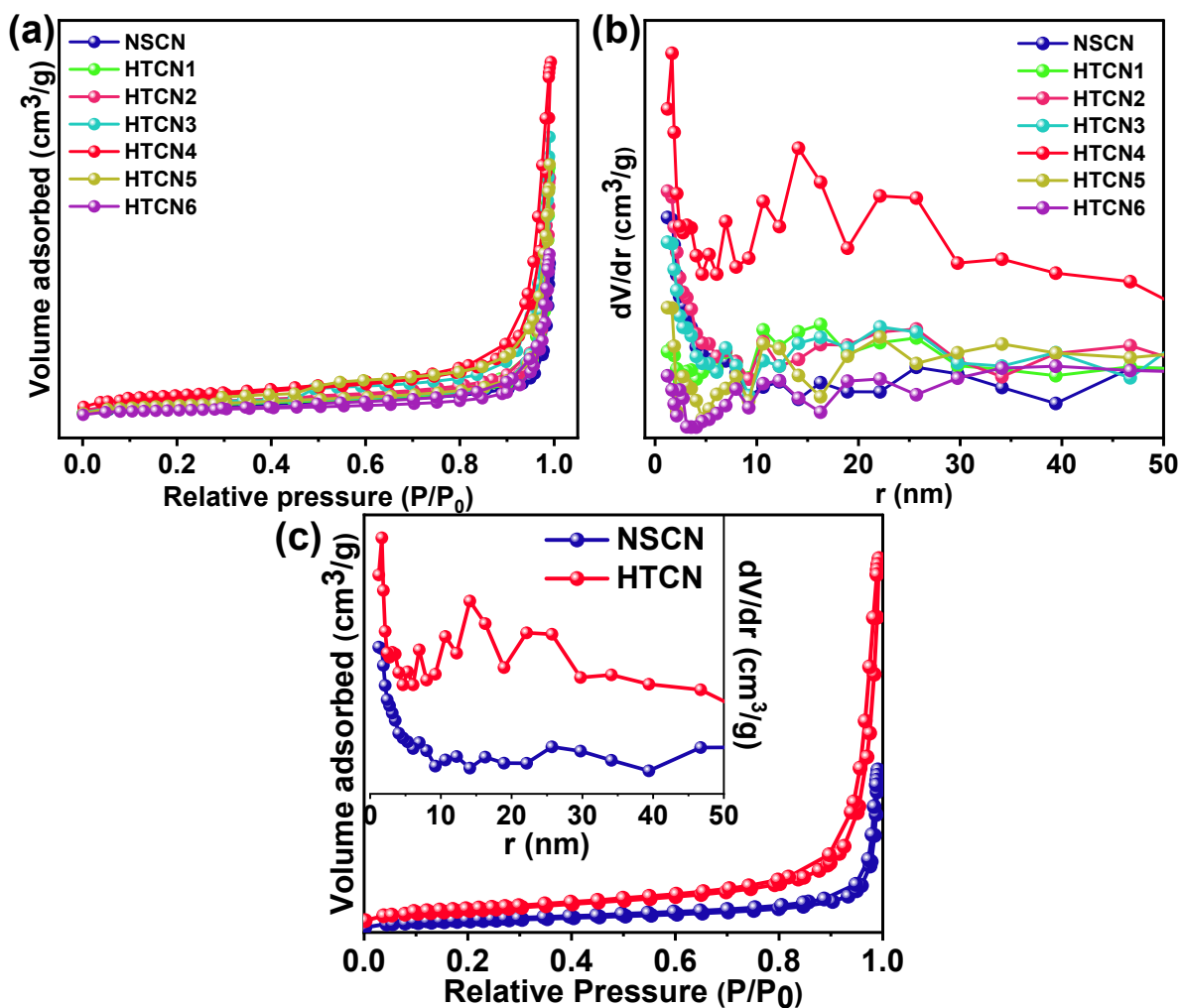


Fig. S2. (a-c) N₂ adsorption-desorption isotherms, BJH pore size distributions of NSCN and HTCN(x).

Table S2. The BET SSA and BJH pore volume of NSCN and HTCN(x).

Catalysts	Surface area (m ² /g)	Pore volume (cm ³ /g)
NSCN	48	0.27
HTCN(1)	54	0.31
HTCN(2)	63	0.43
HTCN(3)	76	0.47
HTCN(4)	92	0.59
HTCN(5)	71	0.36
HTCN(6)	34	0.18

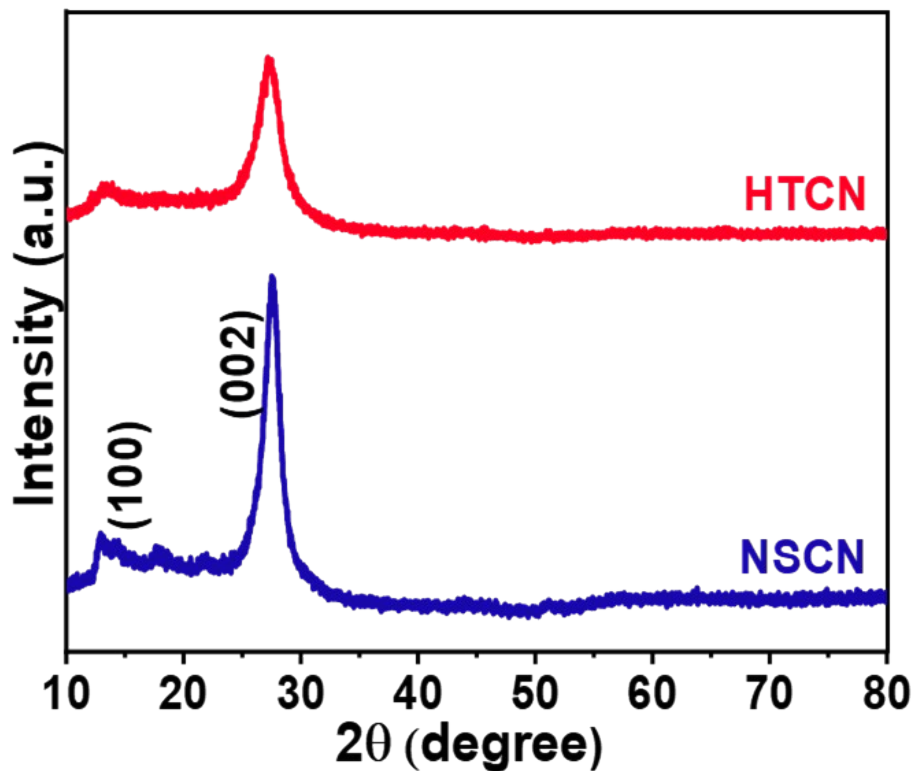


Fig. S3. XRD patterns of NSCN and HTCN.

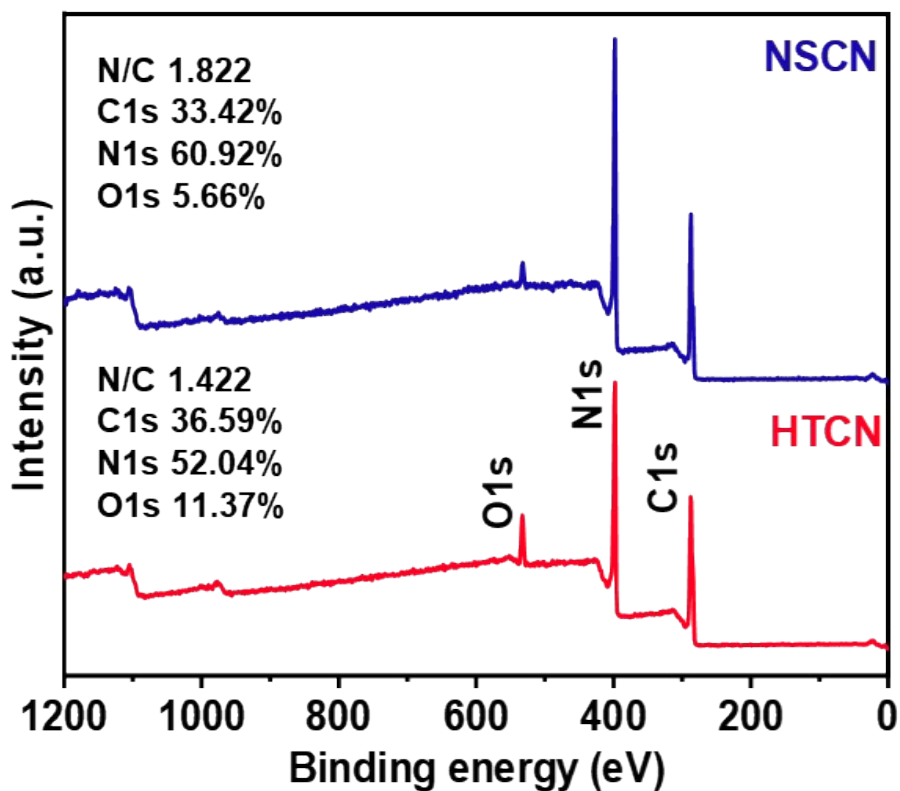


Fig. S4. XPS wide scan survey spectra of NSCN and HTCN.

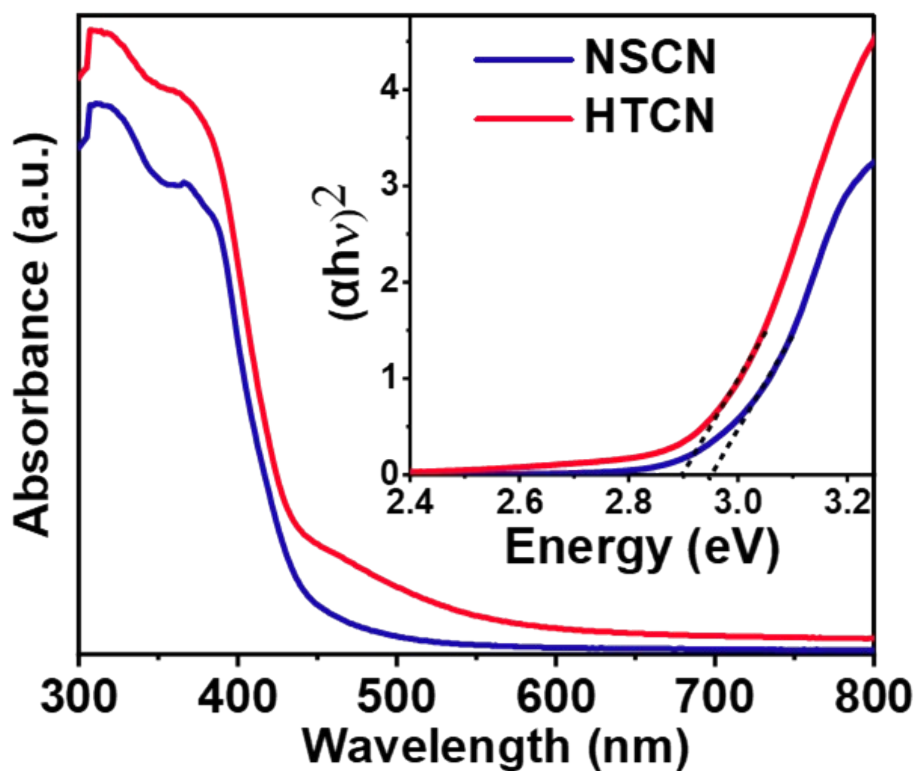


Fig. S5. UV-vis DRS spectra with Tauc plot (inset) of NSCN and HTCN.

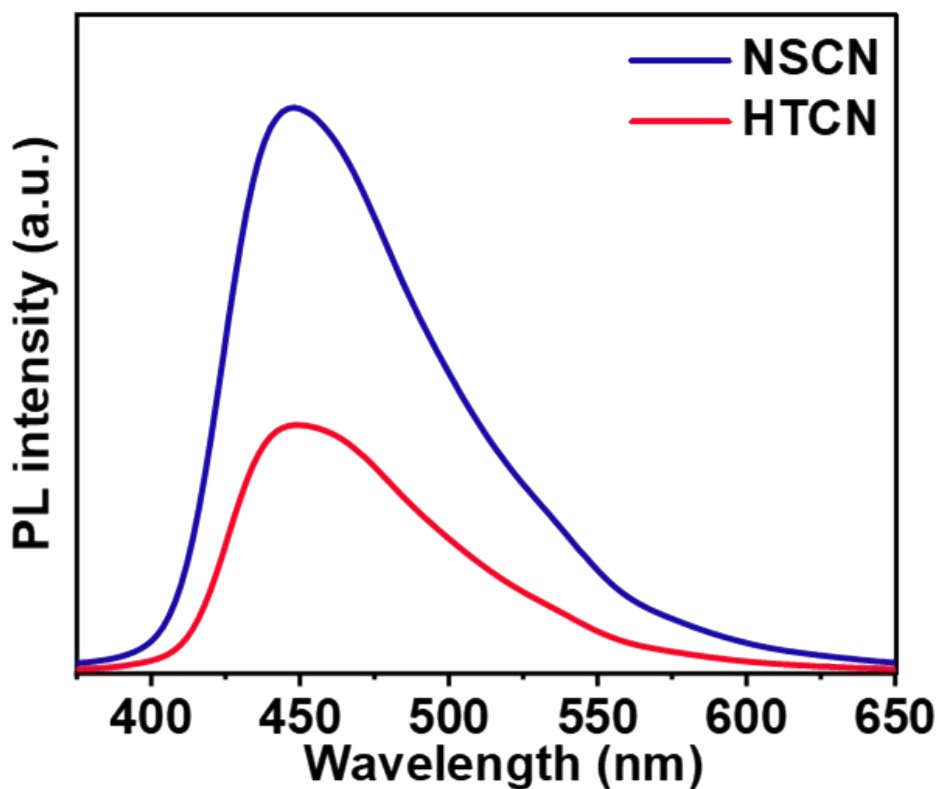


Fig. S6. PL spectra of NSCN and HTCN.

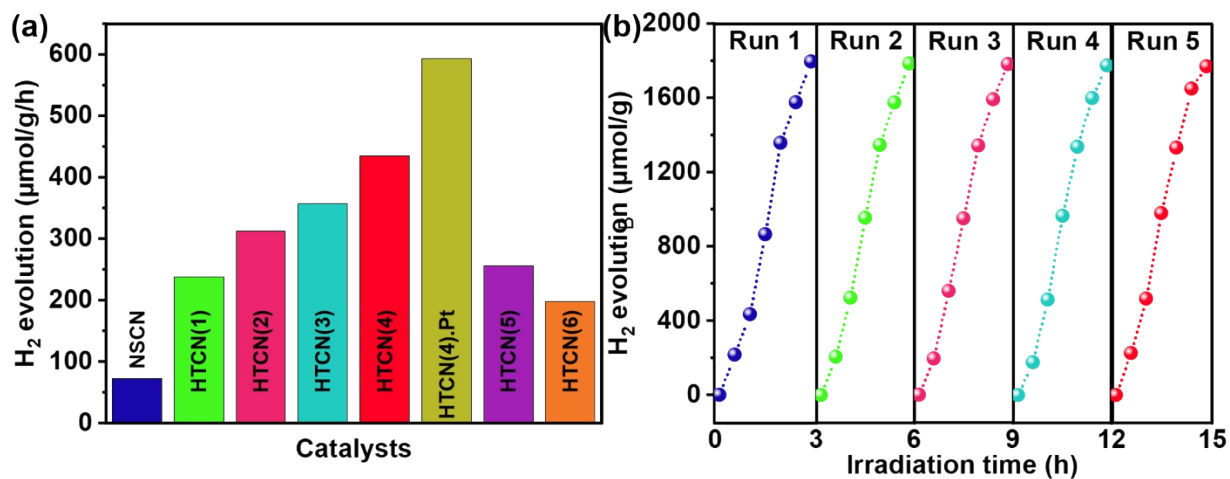
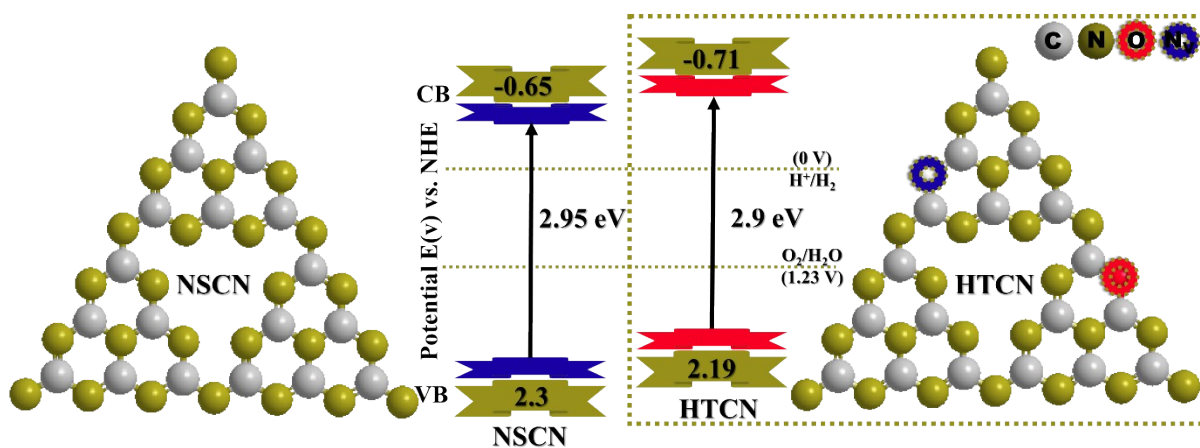


Fig. S7. (a) Comparison of the photocatalytic H₂ evolution rate of NSCN and HTCNC(x).

(b) Cycling test of photocatalytic H₂ evolution of HTCNCatalyst.



Scheme S1. Electronic band structures with schematic illustration of NSCN and HTCNCatalyst.

Table S3. Comparison of synthesis method and photocatalytic performance of varying CN nanotubes.

Catalysts	Synthesis Method	Bandgap (eV)	H₂ Evolution Rate	Ref.
Pt-deposited hexagonal CN nanotubes	Hexagonal precursor rods by Hydrothermal process using bulk CN and further heat-treated to obtain CN nanotubes	2.35	4779.8 $\mu\text{mol/g/h}$ With Pt	1
Halloysite-derived mesoporous CN nanotubes	CN loaded on the acid-treated halloysite templates via a facial melamine-involved vapor deposition method	2.95	633 $\mu\text{mol/g/h}$ With Pt	2
1T'-ReS ₂ nanosheets modified CN nanotubes	CN nanotubes were prepared through the hydrothermal reaction, freeze-drying and heat treatment in sequence	2.34	61 $\mu\text{mol/g/h}$	3
CN tubes	Hexagonal columnar crystals assembled by melamine and cyanuric acid were calcined in tube furnace under argon atmosphere	2.67	343.5 $\mu\text{mol/g/h}$ With Pt	4
g-C ₃ N ₄ microrods	Bulk structure of g-C ₃ N ₄ was degraded into nanoporous microrods via chemical means at room temperature	2.72	8.5 $\mu\text{mol/g/h}$	5
Hierarchical porous CN hollow nanotubes	Thermal polycondensation of oxalic acid-assisted urea and melamine supramolecular aggregates	2.9	435 $\mu\text{mol/g/h}$ Without Pt	Current Work

References

1. Z. Jiang, C. Jia, B. Wang, P. Yang and G. Gao, *J. Alloys Compd.*, 2020, 826, 154145.
2. W. Wang, Z. Shu, J. Zhou, T. Li, P. Duan, Z. Zhao, Y. Tan, C. Xie and S. Cui, *Appl. Clay Sci.*, 2018, 158, 143–149.
3. X. Wang, Y. Xue, Z. Liang, J. Tian, X. Zhang and X. Chen, *Mater. Today Adv.*, 2022, 15, 100257.
4. Yang, B., Han, J., Zhang, Q., Liao, G., Cheng, W., Ge, G., Liu, J., Yang, X., Wang, R. and Jia, X., *Carbon*, 2023, 202, 348-357.
5. Pawar, R.C., Kang, S., Park, J.H., Kim, J.H., Ahn, S. and Lee, C.S., *Scientific reports*, 2016, 6(1), 31147.